THE ASTROPHYSICAL JOURNAL, 395:540–552, 1992 August 20

PULSAR NEBULAE IN SUPERNOVAE

ROGER A. CHEVALIER
Department of Astronomy, University of Virginia, P.O. Box 3818, Charlottesville, VA 22903
AND
CLAES FRANSSON
Stockholm Observatory, S-133 36 Saltsjöbaden, Sweden
Received 1992 January 23; accepted 1992 February 26

ABSTRACT

Pulsars are expected to be born inside Type II supernovae, and the nebulae generated by their spin-down power thus initially interact with the expanding supernova gas. The hydrodynamic interaction can be described analytically while the pulsar is in a constant power output phase if the surrounding density profile is a power law in radius. The power generated by the shock front driven into the supernova gas is about 1.5% of the pulsar power, and, for typical parameters, the shock wave remains in a radiative phase for at least hundreds of years. The stability of the accelerating shell can be analyzed on the thin shell approximation, and we find that linear spherical harmonic perturbations with $l \geq 4$ are unstable to Rayleigh-Taylor instability growth. The growth is exponential in time for large wavenumbers. If the pulsar bubble produces ionizing radiation, the radiation is trapped close to the shocked shell throughout the initial evolution and may be able to break out of the supernova gas only after tens of years. By allowing for the evolution of the pulsar power on the assumption of constant braking index, the model is applied to the young pulsars PSR 0531+21 (Crab), PSR 0540−69, and PSR 1509−58, and their associated nebulae. There is general agreement between the predicted and observed properties of the shell nebulae, and the models make predictions for future observations. If pulsars "turn-on" rapidly after the supernova explosion, our model has implications for observations of supernovae at an age of years. We present detailed results for the possible photoionization in a supernova at ages of 4 and 10 yr. The upper limit on the total power of a pulsar in SN 1987A is $\sim 5 \times 10^{38}$ ergs s^{-1}, or lower if the pulsar nebula has a high radiative efficiency. A general prediction of the pulsar model is broadening of the lines with time because of the acceleration by the pulsar bubble.

Subject headings: pulsars: general — shock waves — supernova remnants

1. INTRODUCTION

The early evolution of pulsars and their interaction with supernova gas remains obscure. The youngest known pulsars are the 33 ms Crab pulsar, the 50 ms pulsar in the Large Magellanic Cloud supernova remnant 0540−69, and the 150 ms pulsar PSR 1509−58, all of which have estimated ages of $\sim 10^3$ yr. There is considerable uncertainty regarding the initial properties of pulsars: it has been proposed that their magnetic fields are built up on a time scale of perhaps hundreds of years (Blandford, Applegate, & Hernquist 1983), and the initial spin rates of typical pulsars remains a controversial topic (Emmering & Chevalier 1989; Narayan & Ostriker 1990). There is general agreement that the place to look for young pulsars is in Type II supernovae, but the effects of large distance and obscuration by the expanding supernova gas make it difficult to directly observe a pulsed source. Upper limits have been set on pulsed optical emission from Type II supernovae (Middleditch & Kristian 1984), but they do not rule out the presence of moderately powerful pulsars.

The Crab Nebula is much more easily visible than the central pulsar, which suggests that a search for young pulsar nebulae could be fruitful. Bandiera, Pacini, & Salvati (1984) suggested that the radio emission observed from some Type II supernovae is pulsar-related, but the current evidence favors the circumstellar interaction model for this emission (Weiler et al. 1986). While radio nebulae are expected around pulsars, they are likely to be obscured by surrounding ionized gas during the early phases of evolution (Reynolds & Chevalier 1984). Optical emission is less likely to be obscured by the expanding gas, and it is that emission that is emphasized in the present work.

Our model for the expanding pulsar nebula in the supernova builds on previous work in this area. Ostriker & Gunn (1971) proposed a model in which the pulsar bubble is the primary mechanism for the supernova explosion. More recent supernova modeling has made clear that there is an initial explosion that shock accelerates the stellar material and the pulsar is embedded within the expanding gas. This has led to a model in which the pulsar bubble expands into uniformly expanding gas (Chevalier 1977; Gaffet 1977). Chevalier (1977) concentrated on the Crab Nebula and suggested a supernova model in which there is separate expansion of core region and an envelope shell. More recent work suggests that there is not a well-defined separation between the core and envelope matter and the more uniform model is taken here.

While some radiation is expected from shock waves driven by the pulsar bubble, the Crab Nebula shows that photoionization can be the dominant source of optical line emission (Davidson & Fesen 1985). Photoionization must be especially important at early times when the expanding supernova gas absorbs most of the ionizing radiation. We therefore calculate the photoionization properties of supernovae in the 4 to 10 yr old range in detail.

In this paper, we develop the theory for pulsar nebulae in supernovae in § 2. In § 3, we apply the theory both to young nebulae known to contain pulsars and to supernovae in which pulsars might be observed. The results are discussed and summarized in § 4.

1992ApJ...395..540C

2. PULSAR NEBULAE

2.1. *Pulsar Surroundings*

When a neutron star first forms in a supernova, continued fallback of matter that is marginally bound to the neutron star may occur (Colgate 1971). Chevalier (1989, 1991) found that during the first 6 months to year after a supernova explosion, the matter accretion is so large that no pulsar effects are possible. After this time, there is a small mass, radiation pressure supported envelope around the neutron star. This envelope may be subject to dynamical instability and after it has dissipated, the newly formed pulsar nebula can begin to interact with the expanding supernova gas (Chevalier 1991).

The density structure of the supernova gas is determined by the initial stellar structure, as modified by the explosion. The density structure has been well determined for models of SN 1987A; it shows an inner flat profile outside of which is a steep power-law decrease with radius (Arnett 1988; Shigeyama & Nomoto 1990). Chevalier & Soker (1989) approximated the velocity profile by an inner section $\rho_i = Ar^{-m}t^{m-3}$ and an outer section $\rho_0 = Br^{-n}t^{n-3}$, where $m = 1$ and $n = 9$ for SN 1987A. Chevalier & Soker argue that a steep power law can be expected under rather general conditions for the outer section provided that radiative losses are not important. The two parts of the density profile are assumed to be continuous and they intersect at a velocity v_t. For an explosion with a total energy E and mass M_t, we have

$$v_t = \left[\frac{2(5-m)(n-5)}{(3-m)(n-3)}\,\frac{E}{M_t}\right]^{1/2} , \tag{2.1}$$

$$A = \left(\frac{n-3}{n-m}\right)\left[\frac{(3-m)(n-3)}{2(5-m)(n-5)}\,\frac{M_t}{E}\right]^{(3-m)/2}\frac{(3-m)M_t}{4\pi} . \tag{2.2}$$

SN 1987A was an unusual Type II supernova because of its small initial radius. More typical Type II supernovae are expected to have red supergiant progenitors and their final density distributions are not well determined. Chevalier (1977) took a core-envelope structure, based on simple hydrodynamic models, and Weaver & Woosley (1980) did find the formation of dense core matter in a shell in more detailed models. However, it is likely that hydrodynamic instabilities, similar to those believed to occur in SN 1987A (Fryxell, Müller, & Arnett 1991), lead to mixing and smooth out any sharp features in the density profile. Chevalier (1977) suggested that the mixture of H and He observed in the Crab Nebula is the result of such instabilities during the explosion of SN 1054. Thus, a reasonably smooth, flat inner density profile may be a good approximation. In the outer part of the density profile, radiative transfer effects are more important for the explosion of an extended star and can lead to the formation of a dense shell in the outer layers. However, the shell is expected out in the steep power-law region of the density profile, where the pulsar bubble is not likely to reach. The two power-law approximation described above may give an adequate representation of the density law. In what follows, we typically take $m = 0$ or 1 and $n = 9$, although more general cases are also discussed.

2.2. *Hydrodynamic Evolution*

We assume that the spin-down energy of the pulsar goes into a bubble of relativistic particles and magnetic field surrounding the pulsar. The bubble shocks and sweeps up the surrounding supernova gas. In previous models of this type (Ostriker & Gunn 1971; Chevalier 1977), it has been assumed that the bubble interior can be treated as a uniform isotropic relativistic fluid with $\gamma = 4/3$. However, a substantial part of the energy is expected to go into the magnetic field, which can form a toroidal structure surrounding the pulsar (Rees & Gunn 1974; Kennel & Coroniti 1984a). The pressure is then not isotropic and the effective γ in the radial direction is greater than 4/3. In the model of Kennel & Coroniti (1984a) for the Crab Nebula, the tangential component of the magnetic field drops as $1/r$ at large radii r and the magnetic field pressure is dominant. Emmering & Chevalier (1987) considered self-similar models for the Crab Nebula in which the outer boundary moves at constant velocity. They calculated models with the same total energy input, L, but different percentages of relativistic particle and magnetic field components, and showed that the pressure at the outer boundary is always the same, equivalent to the uniform relativistic fluid case. In cases with a high magnetic field, the average pressure is higher for a given total internal energy, but this is balanced by the gradient in the magnetic field. In what follows, we assume that the bubble interior can be treated as a uniform fluid with $\gamma = 4/3$.

With the further assumption that the supernova gas is swept into a thin shell of mass M, radius R, and velocity V, the evolution of the shell is described by (Ostriker & Gunn 1971; Chevalier 1977)

$$M\,\frac{dV}{dt} = 4\pi R^2[p_i - \rho_e(V - v_e)^2] , \tag{2.3}$$

$$\frac{d(4\pi R^3 p_i)}{dt} = L - p_i 4\pi R^2\,\frac{dR}{dt} , \tag{2.4}$$

where p_i is the pressure at the outer edge of the bubble and ρ_e and v_e are the supernova density and velocity just external to the shell.

The pulsar power output is $L = I\Omega\dot{\Omega}$, where I is the neutron star moment of inertia and Ω is its spin rate. A commonly assumed form for the evolution of Ω is $\dot{\Omega} = -f\Omega^b$, where $b = 3$ for a vacuum dipole rotator and can be less than 3 if there is a substantial particle wind. The function f is constant with time if the magnetic moment is constant, in which case $b = \Omega\ddot{\Omega}/\dot{\Omega}^2$ is the braking index. Assuming constant b and f over the evolution leads to

$$L = \frac{L_0}{(1 + t/\tau)^{(b+1)/(b-1)}} , \tag{2.5}$$

where L_0 is the initial power output and τ is a time scale.

If $t < \tau$, the power output is approximately constant at L_0 and it is straightforward to solve equations (2.3) and (2.4) taking ρ_e to be the inner density profile ρ_i and $v_e = r/t$, as expected in free expansion. The solution of the dynamical equations is then

$$R = \left[\frac{(5-m)^3(3-m)}{(11-2m)(9-2m)}\,\frac{L_0}{4\pi A}\right]^{1/(5-m)} t^{(6-m)/(5-m)} . \tag{2.6}$$

It can be seen that the solutions are applicable only for $m < 3$, which is equivalent to the requirement of finite mass in the shell. The energetics of the expansion are as follows. The thin shell approximation is equivalent to the assumption that the shock front is radiative, so the radiated energy is

$$E_{\rm rad} = \int_0^t 4\pi R^2\,\frac{1}{2}\,\rho_e(V - v_e)^3\,dt = \frac{3-m}{2(11-2m)(9-2m)}\,L_0 t . \tag{2.7}$$

1992ApJ...395..540C

The internal energy in the bubble is

$$E_{\rm int} = 4\pi R^3 p_i = \frac{5-m}{11-2m} L_0 t\ , \tag{2.8}$$

and the kinetic energy of the shell is

$$E_{\rm kin} = \frac{1}{2} M V^2 = \frac{(5-m)(6-m)^2}{2(11-2m)(9-2m)} L_0 t\ . \tag{2.9}$$

The energies for various values of m are given in Table 1, which also includes z, the exponent of t in equation (2.6), and $E_{\rm sw}$, the kinetic energy that is added to the shell by the preshock expansion of the gas. We note that $L_0 t = E_{\rm rad} + E_{\rm int} + E_{\rm kin} - E_{\rm sw}$ by energy conservation. In the limit $m \rightarrow 3$, the expansion exponent and the energetics approach the case of the acceleration of a constant mass shell (Ostriker & Gunn 1971). These results are exact for the case that all of the shock energy is radiated, but they are also quite accurate for the case in which energy is conserved in the postshock region because the shocked shell is thin in the nonradiative case. Chevalier (1984) gives exact results for the nonradiative $m = 0$ case and finds that the shock radius is 3% larger than in the radiative case. The thermal energy in the shocked gas is only $0.006 L_0 t$.

We now consider the solutions for supernova models with $n = 9$ and two values of m, 0 and 1. For $m = 0$, the shell velocity is

$$V = 4.87 \times 10^2 L_{39}^{0.2} E_{51}^{0.3} M_{t1}^{-0.5} t_{\rm yr}^{0.2}\ {\rm km\ s^{-1}}\ , \tag{2.10}$$

where L_{39} is L_0 in units of 10^{39} ergs s^{-1}, E_{51} is E in units of 10^{51} ergs, M_{t1} is the mass M_t in units of 10 $M_\odot$, and $t_{\rm yr}$ is the age in years. The shock velocity into the supernova gas is $V/6$. The time that it takes V to reach the density transition velocity v_t is $3.7 \times 10^4 E_{51}/L_{39}$ yr, so it is likely that the shell remains within the inner part of the density profile during the constant power output phase. Radiative cooling of the shocked gas is expected to be important at early times when the external density is high, and to become no longer important at a time, t_c, when the cooling time is equal to the age. From the results in McKee & Hollenbach (1980) for shock velocities in the range 60–1000 km s^{-1}, we find $t_c = 320 L_{39}^{-0.24} E_{51}^{-0.93} M_{t1}^{1.55} \alpha^{0.38}$ yr, where α is a factor to account for the increased cooling rates that might be expected because of enhanced heavy-element abundances above the cosmic abundances assumed in the shock models. For the $m = 1$ case we find

$$V = 2.89 \times 10^2 L_{39}^{0.25} E_{51}^{0.25} M_{t1}^{-0.5} t_{\rm yr}^{0.25}\ {\rm km\ s^{-1}}\ , \tag{2.11}$$

and the shock velocity is $V/5$. The time that it takes V to reach v_t is again long, $6.3 \times 10^4 E_{51}/L_{39}$ yr. The end of the cooling phase occurs at $t_c = 430 L_{39}^{-0.35} E_{51}^{-0.67} M_{t1}^{1,34} \alpha^{0.33}$ yr.

When the variation of L with t is taken into account, numerical integration of the dynamical equations must typically be performed (see § 3). However, some insight can be obtained by considering the case of $L \propto t^{-\beta}$. The resulting expansion law is $R \propto t^{(6-m-\beta)/(5-m)}$. Constant velocity expansion is obtained for $\beta = 1$ and is expected for all $\beta > 1$ because the shell must expand at least at this rate. The reason is that all the energy is injected at an early time. If $\beta < 1$ initially, the shell will continue to accelerate in the $\beta > 1$ regime, but should gradually tend toward free expansion.

TABLE 1

ENERGETICS

m	z	$E_{\rm rad}/Lt$	$E_{\rm int}/Lt$	$E_{\rm kin}/Lt$	$E_{\rm sw}/Lt$
0.........	1.2	0.01515	0.4545	0.9091	0.3788
1.........	1.25	0.01587	0.4444	0.7937	0.2540
2.........	1.33	0.01429	0.4286	0.6857	0.1286
3.........	1.5	0.0	0.4000	0.6000	0.0

Finally, we consider the case where the pulsar suddenly turns on with power L_0 at time t_0. This time might be determined by the end of a phase of dense neutron star accretion or by the sudden increase of the neutron star magnetic field. Provided that $(t - t_0) \ll t$, the supernova gas is effectively time independent, with $v_e = 0$. The solution of the dynamical equations is then given by

$$R = \left[\frac{(3-m)(5-m)^3}{3(7-2m)(8-m)} \frac{L_0}{4\pi A}\right]^{1/(5-m)} (t - t_0)^{3/(5-m)}\ . \tag{2.12}$$

This solution is similar to that for a stellar wind driven bubble (Weaver et al. 1977) except that $\gamma = 4/3$ for the present case and is 5/3 for the stellar case. A difference with the uniform expansion case is that the radiated luminosity is

$$L_{\rm rad} = \frac{9(3-m)}{2(7-2m)(8-m)} L_0 \tag{2.13}$$

and is a substantial fraction of L_0. We have $L_{\rm rad}/L_0 = 0.241$, 0.247, 0.250 for $m = 0, 1, 2$, respectively.

2.3. *Shell Stability*

The expansion of a thin shell subject to interior pressure forces can be examined for stability. Vishniac (1983) has already studied the case of expansion into a stationary, uniform medium; the major difference here is that the external medium has a changing density and a velocity field. Vishniac did find that the stability could be simply analyzed for an infinitely thin, planar shock if all terms that enter only on time scales comparable to the age of the shock are dropped. Then a linear perturbation to the surface density σ, of the form $\delta \propto \exp(\Gamma t_1 + i\boldsymbol{k} \cdot \boldsymbol{x})$ leads to

$$\Gamma = (p_i k^2 \dot{V}/\sigma)^{1/4}\ , \tag{2.14}$$

where t_1 is measured from the beginning of the instability growth and is $\ll t$. For an accelerating shell ($\dot{V} > 0$), there is growth of the Rayleigh-Taylor instability. The differences of the present case with that studied by Vishniac involve terms that evolve on time scales comparable to the age of the shock, so that equation (2.14) can be applied here for the case of large k. The solution described by equation (2.14) leads to

$$\Gamma = [(6-m)(9-2m)]^{1/4} \frac{(kR)^{1/2}}{(5-m)t}\ . \tag{2.15}$$

The coefficient of $(kR)^{1/2}/t$ is 0.542, 0.608, 0.705, and 0.866 for $m = 0$, 1, 2, and 3, respectively. Exponential growth of the instability occurs at large kR at a rate that does not strongly depend on m.

While rapid growth can occur at small scales in the linear regime, these scales are also the ones where the instability saturates first and it is likely that the dominant structure appears on the largest scales that are able to grow. These scales can be found from a full analysis of the shell stability along the lines of the analysis by Vishniac (1983). We have considered two cases with constant power input: expansion into uniformly expanding gas with a uniform density ($m = 0$) and expansion of a constant mass shell. The analysis is carried out for a general power-law expansion, $R_0 \propto t^w$, where R_0 is the unperturbed radius, although the two cases are characterized by $w = 1.2$ and 1.5, respectively. The perturbed variables are $\delta = \sigma/\sigma_0 - 1$, where σ_0 is the unperturbed surface density, $\Delta R = R - R_0$, and V_{T}, which is the tangential velocity mass averaged over the shell thickness. For the first case (uniform external expansion), the solution takes the form

$$\delta = \delta_0(t/t_0)^s Y_{lm} , \qquad (2.16)$$

$$\Delta R = w(1-w)[(s+w)(s+7w-7)]^{-1} R_0 \delta_0(t/t_0)^s Y_{lm} , \qquad (2.17)$$

$$V_{\mathrm{T}} = (4w-3)w(w-1)^2[(s+w)(s+7w-7) \times (s+6w-4)]^{-1}(R_0^2/t)\delta_0(t/t_0)^s \nabla_{\mathrm{T}} Y_{lm} , \qquad (2.18)$$

where

$$(s+6w-4)[(s+w)(s+3w-3)(s+7w-7) - (s+3w)w(1-w)] = w(w-1)^2(4w-3)l(l+1) , \qquad (2.19)$$

and the Y_{lm} are the usual spherical harmonics. With $w = 1.2$, the critical l for instability ($s = 0$) is $l_c = 4.97$. This is the limiting minimum value of l for which instability growth can occur. For the second case (constant shell mass), the solution takes the form

$$\delta = \delta_0(t/t_0)^s Y_{lm} , \qquad (2.20)$$

$$\Delta R = w(1-w)[(s+w)(s+w-1)]^{-1} R_0 \delta_0(t/t_0)^s Y_{lm} , \qquad (2.21)$$

$$V_{\mathrm{T}} = w^2(w-1)^2[(s+w)(s+w-1)(s+3w-1)]^{-1} \times (R_0^2/t)\delta_0(t/t_0)^s \nabla_{\mathrm{T}} Y_{lm} , \qquad (2.22)$$

where

$$(s+3w-1)[s(s+w)(s+w-1) - (s+3w)w(1-w)] = w^2(w-1)^2(4w-3)l(l+1) . \qquad (2.23)$$

With $w = 1.5$, the critical l for instability is $l_c = 4.11$. We note that the spherical harmonics are defined such that the value of l gives the number of minima in R in a great circle taken around the shell.

2.4. *Photoionization*

It is plausible that emission from the pulsar bubble provides a larger luminosity source than the radiative shock front. Kennel & Coroniti (1984b) have discussed a magnetohydrodynamic model for the high-energy emission from the Crab Nebula, but the model depends on the magnetization parameter and velocity of the pulsar wind and the spectra index of shocked electrons and positrons. These parameters are determined from observations of the Crab Nebula and are not known for cases of younger pulsars. Seward & Wang (1988) summarize the data on X-ray emission from pulsar nebulae and note that the efficiency of X-ray production for the three pulsar nebulae mentioned in § 1 is high, greater than $0.01L$ for all the cases. If this is a general property of the nebulae around more energetic pulsars, the bubble emission can be expected to dominate the shock emission for the cases of interest here. This is particularly important for the young supernovae, because the ionizing radiation is absorbed within the supernova gas. Here we assume that a fraction f_i of the total power L is emitted in the form of ionizing radiation with a mean free path that is small compared to the supernova size. Some other fraction of L may be emitted in hard radiation that is able to partially ionize the supernova. The softer radiation is able to ionize a region of radius R_i determined by

$$\frac{f_i L}{\zeta I_{\mathrm{H}}} = \frac{4}{3}\pi R_i^3 n_e n_A \alpha_r , \qquad (2.24)$$

where I_{H} is the ionization potential for hydrogen, n_e is the electron density, n_A is the density of heavy particles, α_r is the recombination coefficient, and

$$\zeta I_{\mathrm{H}} = \frac{\int_{\nu 0}^{\infty} J_\nu d\nu}{\int_{\nu 0}^{\infty} (J_\nu d\nu/h\nu)} \qquad (2.25)$$

is the effective energy needed per ionization, which depends on the shape of the ionizing spectrum, J_ν, and the threshold energy, $h\nu_0$. Taking $\alpha_r = 3 \times 10^{-13} A_r$ cm^3 s^{-1} and the density distribution appropriate to the $m = 0$, $n = 9$ model described above, we have

$$R_i = 2.82 \times 10^{14}(f_i \mu^2/\zeta B_e A_r)^{1/3} L_{39}^{1/3} M_{t1}^{-5/3} E_{51} t_{\mathrm{yr}}^2 \text{ cm} , \qquad (2.26)$$

where μ is the atomic weight in amu, B_e is the number of electrons per atom, and it is assumed that R_i occurs in the flat part of the density profile. This expression does not take into account the fact that the pulsar nebula sweeps up the surrounding supernova gas. Although the density of the shell is high and is potentially capable of strong absorption of the photoionizing radiation, the shell is subject to the Rayleigh-Taylor instability, so we assume that most of the shell mass ends up in filaments with a small covering factor (as in the Crab Nebula) and the ionizing radiation penetrates directly into the supernova. If the bubble radius R is greater than R_i, then the radiation is able to photoionize only a small region out ahead of R. If $R_i > R$, then the estimate of R_i is applicable. The time scale for the transition to occur is

$$t_{\mathrm{yr}} = 6.6(\zeta B_e A_r/f_i \mu^2)^{0.42} L_{39}^{-0.17} M_{t1}^{1.46} E_{51}^{-0.88} . \qquad (2.27)$$

Eventually the ionization front reaches the edge of the constant density region and the steep power-law part of the density profile is rapidly ionized. This occurs at a time

$$t_{\mathrm{yr}} = 48(\zeta B_e A_r/f_i \mu^2)^{1/3} L_{39}^{-1/3} M_{t1}^{7/6} E_{51}^{-1/2} . \qquad (2.28)$$

The constant $t_0 = 48(\zeta B_e A_r/f_i \mu^2)^{1/3}$ depends on the composition of the core and the efficiency f_i. For a hydrogen-dominated core $t_0 = 79 f_i^{-1/3}$, for a helium-dominated core $t_0 = 32 f_i^{-1/3}$, and for an oxygen-dominated core $t_0 = 13.2 f_i^{-1/3}$.

In Figure 1 we show the velocity of the ionization front and the outer boundary of the pulsar bubble for these three compositions, and a core with mass 4 $M_\odot$ and velocity 2000 km s^{-1}. We have assumed an ionizing spectrum of the same form as the Crab (Davidson & Fesen 1985), with a luminosity $f_i L = 1 \times 10^{39}$ ergs s^{-1} above 13.6 eV, and an efficiency $f_i = 0.3$. This may correspond to the Crab during the first decades after the explosion. In this simple model the line emission is expected to be confined to the region between the pulsar bubble and the ionization front. The line profile should therefore be flat for velocities less than the bubble velocity, and the maximum velocity of the line should increase with time. In a realistic situation, the inhomogeneous structure of the ejecta will probably change this picture substantially. Monitoring the changes in line profiles should be of great interest as a discriminator between the pulsar photoionization scenario, circumstellar excitation, and shock emission from the bubble interaction. In the circumstellar case the lines are expected to have a velocity

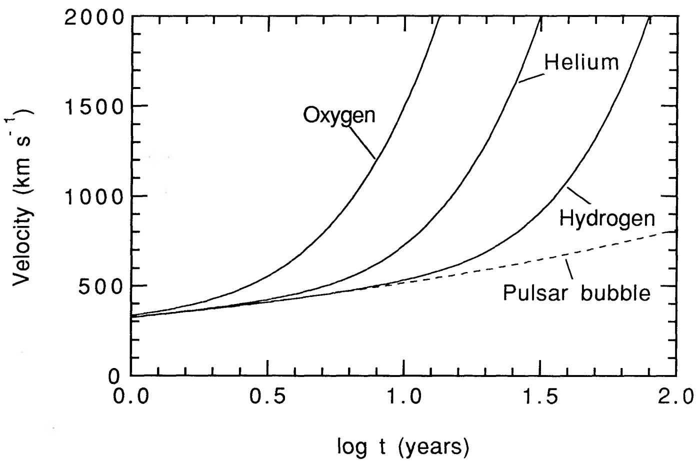

FIG. 1.—Velocities of the outer boundary of the pulsar bubble and the ionization fronts for hydrogen, helium, and oxygen-dominated cores. The parameters of the model are given in the text.

of ~5000 km s^{-1}, decreasing with time, while the emission from the bubble shock is expected to have a slow increase in velocity with time.

2.5. *Spectral Characteristics*

To examine the spectral signatures of the pulsar excitation we have calculated a number of detailed photoionization models for the structure of the pulsar nebula. Calculations for γ-ray excited remnants have already been carried out for up to ~3 yr after the explosion (Fransson & Chevalier 1987, 1989). Because of the large penetrating power of the γ-rays, the ionizing secondary electrons are in this case fairly uniformly distributed, and it was found that the conditions do not vary dramatically throughout the remnant, except as a result of abundance changes. Consequently, the resulting ionization is low, and the strongest lines come from neutral and singly ionized species, like H I, C I, O I, Mg I, Ca II. In the case of pulsar excitation most of the energy is emitted at comparatively low energies, where photoelectric absorption is high. Therefore, the radiation will ionize gas only in a shell close to the ionizing source, unless the density is low. The result is a thin zone of comparatively high ionization, and an extended low-ionization zone excited by keV photons. This structure is similar to the broad line regions of active galactic nuclei.

The calculations use an updated version of a code earlier employed for γ-ray excited supernova ejecta and galactic halo calculations (Fransson & Chevalier 1985, 1989). This includes a detailed multilevel treatment of hydrogen with five bound levels, He I with 16 levels, O I with nine levels, and Ca II with four levels. In the oxygen-rich models, recombination emission from O I–IV has to be included. For ordinary recombination we use the approximate emissivities in Borkowski & Shull (1990), and for dielectronic recombination the rates in Nussbaumer & Storey (1984). Charge transfer processes involving H and He with the metals are included, as well as a few reactions among the metals themselves. These can be important for the highly enriched gas in the core. An example is the reaction O II + Ca I → O I + Ca II, which keeps calcium ionized in the oxygen-rich regions in the core. Unfortunately, many rates among the metals are lacking. Photons of high energy create fast, nonthermal electrons in the photoionization process, which are thermalized in the gas. This is calculated using the deposition calculations in Kozma & Fransson (1992). The elements included are H, He, C, N, O, Ne, Na, Mg, Al, Si, S, Ar, Ca, and Fe, with all ionization stages. The recombination time scale for hydrogen is $5.8(n_e/1 \times 10^7 \text{ cm}^{-3})^{-1}$ days, and shorter for other ions. Because $n_e \approx 4.3 \times 10^9 t_{\rm yr}^{-3}$ cm^{-3}, the assumption of ionization and thermal equilibrium is satisfied for at least the first 50 yr, except in regions of very low ionization. These are of less interest here.

The ionizing radiation from the pulsar is assumed to have the same spectral form as the Crab (Davidson & Fesen 1985), and total luminosity of 10^{39} ergs^{-1} between 13.6 eV and 10 keV. The effect of varying the luminosity is discussed below. Instabilities during the explosion, as well as the bubble interaction, makes mixing between different composition zones important. Therefore, the composition and density structure of the core, in particular the region close to the bubble, is highly uncertain. Two-dimensional calculations of the explosion show that even hydrogen can penetrate deep into the core (e.g., Herant & Benz 1992). Mixing is likely to be mainly *macroscopic* with distinct "fingers and blobs" from the different composition zones. This is also the case for the instabilities connected with the pulsar bubble. To examine the effects of a varying composition we discuss three different cases. In model MS the composition is assumed to be solar. In models MHe, and MO we take the composition to be typical for the helium and oxygen core, respectively. A realistic case may be a weighted mean of the spectra from these models. Abundances for these cases are calculated from the 10 H model by Woosley (1988) and are given in Table 2. The density in the core is assumed to be constant ($m = 0$), with the inner boundary set by the bubble radius from equation (2.6). The mass of the expanding core is taken to be 4 $M_\odot$, excluding the neutron star, and the core velocity 2000 km s^{-1}. Outside of the core we assume an $n = 0$ envelope with solar composition. This region is not important at the epochs studied here, because the ionizing radiation does not penetrate into the envelope (see eq. [2.26]). The structure has been calculated for an age of 1500 days (4 yr). Later epochs are discussed in § 2.6. The number density in the core is at 1500 days 5.5×10^7 cm^{-3}, 1.6×10^7 cm^{-3}, and 3.9×10^6 cm^{-3}, for models MS, MHe, and MO, respectively. The outer boundary of the bubble is at 427 km s^{-1} (5.5×10^{15} cm). As argued in § 2.4, we neglect absorption of the ionizing radiation by gas swept up by the bubble.

In Figures 2–4 we show the resulting temperature, ionization structure, and line emissivities as functions of the distance from the pulsar bubble for the three models. To clearly show the contribution of the various lines to the total luminosity, the emissivity is given as $dL/d \log(\Delta r)$. Table 3 gives the luminosities of the strongest lines in the models at 1500 days. Below

TABLE 2

ABUNDANCES BY NUMBER

Element	MS	MHe	MO
H	0.92	0	0
He	7.7×10^{-2}	0.975	0
C	4.1×10^{-4}	1.8×10^{-2}	8.2×10^{-3}
N	1.1×10^{-4}	2.9×10^{-6}	0
O	8.0×10^{-4}	2.0×10^{-3}	0.85
Ne	1.0×10^{-4}	4.0×10^{-3}	4.4×10^{-3}
Mg	3.3×10^{-5}	1.2×10^{-4}	8.9×10^{-5}
Si	4.1×10^{-5}	1.4×10^{-4}	7.8×10^{-2}
S	2.0×10^{-5}	6.8×10^{-5}	4.4×10^{-2}
Ar	8.6×10^{-6}	3.0×10^{-5}	6.3×10^{-3}
Ca	2.4×10^{-6}	8.4×10^{-6}	1.3×10^{-3}
Fe	4.9×10^{-5}	1.7×10^{-4}	4.9×10^{-5}

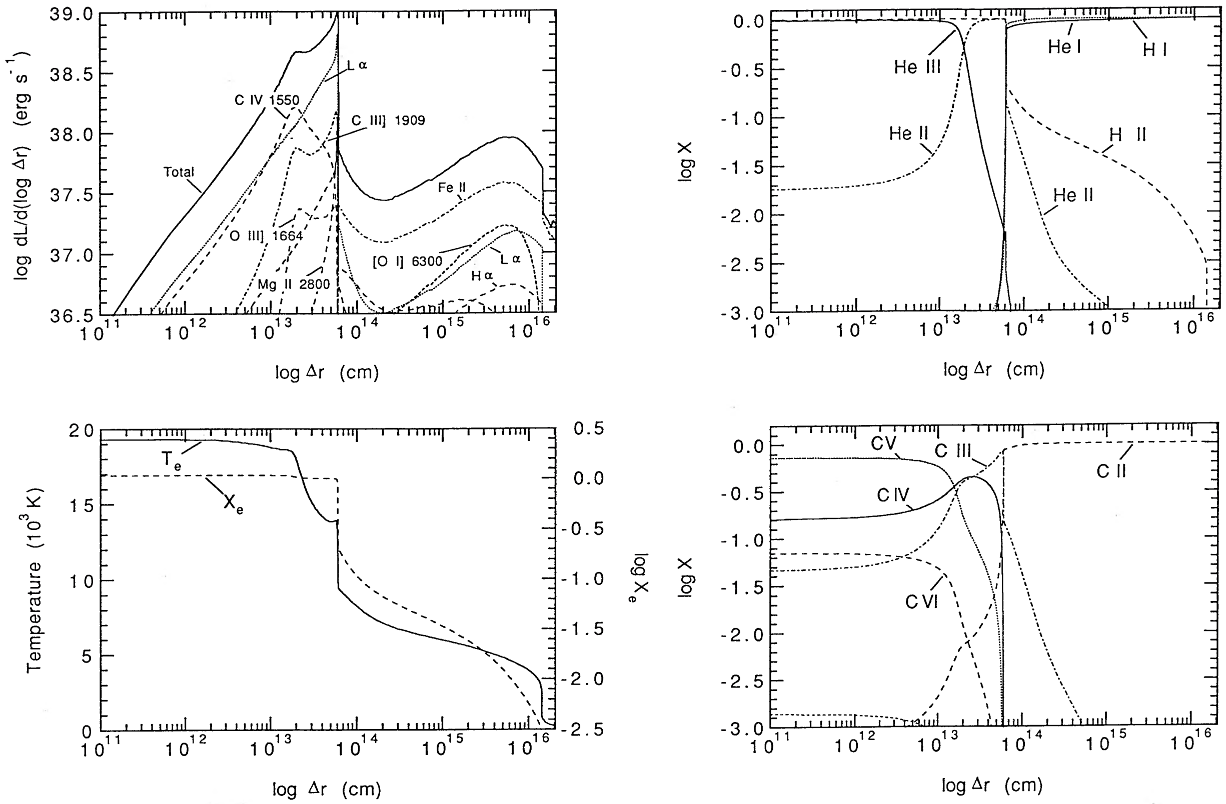

FIG. 2.—Temperature, electron fraction, ionic abundances, and line emissivities as a function of radius for the solar composition core. The emissivity is given as the line luminosity per logarithmic unit radius, *dL*/*d* log Δ*r*. Δ*r* is the distance from the outer boundary of the pulsar bubble.

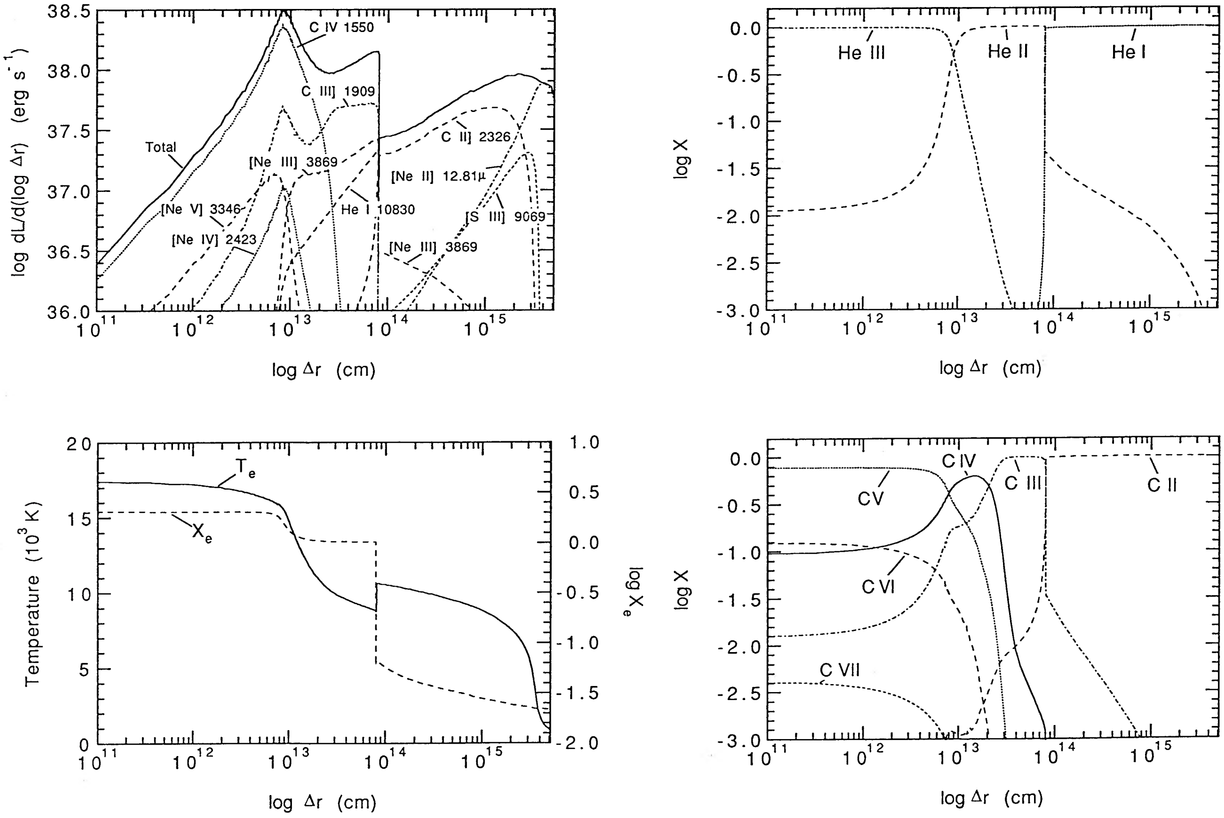

FIG. 3.—Same as Fig. 2 for the helium-dominated core

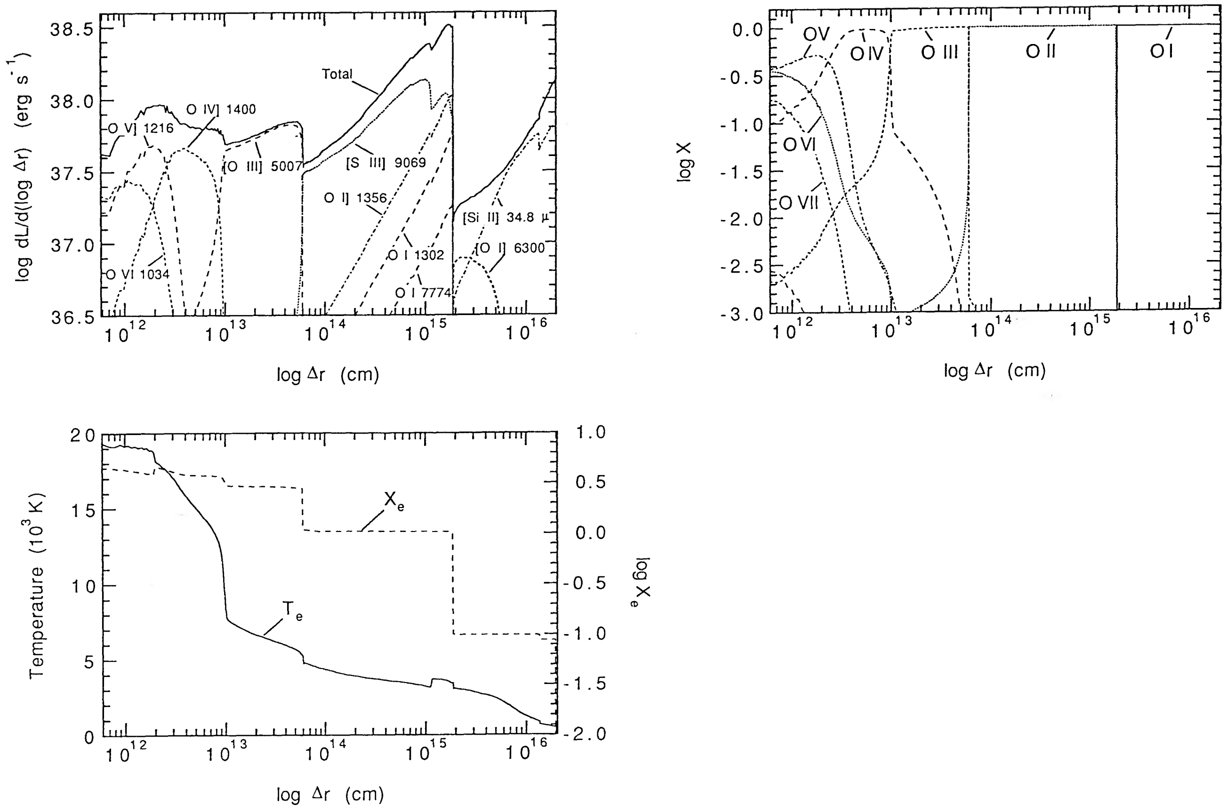

FIG. 4.—Same as Fig. 2 for the oxygen-dominated core

we discuss some of the characteristics of these models and the emission from them.

For a core of solar composition, model MS in Figure 2, the remnant shows a structure typical of emission line regions in active galactic nuclei. The total extent of the ionized region is only $\sim 6 \times 10^{13}$ cm at 1500 days. Near the inner boundary there is a thin, highly ionized region with H II, He III, C V, O IV–VI, with a temperature $\sim$19,000 K, decreasing to $\sim$14,000 K at the He II boundary. Most of the emission is due to Lyα, C IV λ1550 and C III] λ1909. Outside the H II region, the electron fraction decreases slowly from $\sim$0.3 to $\sim 10^{-2}$, and the temperature from $\sim$7000 K to $\sim$3000 K. The strongest lines from this region are [O I] λλ6300–6364, Hα, Lyα, and emission from Fe II. Finally, at 1.45×10^{16} cm the temperature drops rapidly to only $\sim$300 K as fine structure cooling by far-infrared [Fe II] lines cause a thermal instability. This also causes a rapid drop in the electron fraction.

The total emission from this model is dominated by ultraviolet lines of Lyα, C IV λ1550 and C III] λ1909. In the optical, the strongest lines are Hα, [O III] λλ4363, 4959–5007, and [O I] λλ6300–6364. Collision excitation results in a steep Balmer decrement, and the optical depth in the Balmer continuum is 2.8×10^{-3}. Because of the high density, the [O III] λλ4363/4959–5007 ratio is $\sim$1.

The helium core model, MHe in Figure 3, has, as all the other models, a thin, highly ionized He III shell with a temperature of $\sim$16,000 K. Most of the cooling here is by C IV λ1550, C III] λ1909, and [Ne III] λλ3869–3968. The tem-

TABLE 3

LUMINOSITIES[a] OF THE STRONGEST LINES AT 1500 DAYS FOR CORES OF DIFFERENT COMPOSITIONS

MS		MHe		MO	
Lyα	1.84	C IV 1550	1.08	[S III] 9069–9532	1.07
C IV 1550	0.97	C II] 2326	0.48	[O III] 4959–5007	0.46
C III] 1909	0.54	C III] 1909	0.47	O I] 1356	0.36
Hα	0.26	[Ne II] 12.81 μm	0.27	O V] 1216	0.33
[O I] 6300–6364	0.15	[Ne III] 3869–3968	0.18	O VI 1034	0.30
Mg II 2800	0.14	[S III] 9069–9532	0.096	[Si II] 34.81 μm	0.28
O III] 1664	0.12	He II 1640	0.086	O IV] 1400	0.28
O V] 1216	0.070	He I 10830	0.082	O I 1302	0.17
C III 977	0.057	[Ne V] 3346–3426	0.082	O I 7774	0.061
O IV] 1400	0.056	[Ne IV] 2423–2425	0.041	Mg I] 4571	0.053
[O III] 4363	0.051	[O III] 4959–5007	0.024	[Ne II] 12.81 μm	0.046
N IV] 1486	0.049	[O II] 7320–7330	0.016	O I 990	0.045

[a] All luminosities in 10^{38} ergs s^{-1}.

perature then decreases in the He II shell to ~ 9000 K, with cooling dominated by C III] $\lambda1909$, [Ne III] $\lambda\lambda3869$–3968, and He I $\lambda10830$. At $\sim 8 \times 10^{13}$ cm the ionization drops as helium becomes neutral. Because of the high ionization potential of He I, the metals are still ionized, with C II as the most abundant ion; the residual ionization is $\sim 4 \times 10^{-2}$. Cooling is mainly by C II] $\lambda2326$, [Ne II] $\lambda12.81$ μm, and [S III] $\lambda\lambda9069$–9532. At $\sim 4 \times 10^{15}$ cm there is a rapid drop in temperature as fine structure cooling by especially [Ne II] $\lambda12.81$ μm becomes dominant. The total emission from the helium shell gas reflects the abundances fairly well, except for helium itself, with ultraviolet emission from C IV, C III], and C II] dominating. The great strength of the neon lines is a consequence of the fairly high neon abundance in the helium zone, $\sim 5 \times 10^{-3}$. In the optical range [S III] $\lambda\lambda9069$–9532 and [Ne III] $\lambda\lambda3860$–3968 are especially strong. The strongest helium line is the $\lambda10830$ line, which is enhanced by collisional excitation. The spectrum is similar to the solar case, except for the absence of hydrogen lines. Mixtures of hydrogen-rich and helium-rich gas give similar results, except for the recombination lines. The main diagnostic of a helium enrichment is a large He I to H I recombination line ratio. The metal abundances in the helium zone are uncertain, because they depend on convective mixing in the progenitor, so the exact results are model dependent, especially for elements beyond oxygen.

At the inner boundary of the oxygen core model (Fig. 4), the dominant ions are O IV–O VI, all with strong ultraviolet lines. The temperature here is 15,000–19,000 K. Next comes a thin O III zone, with $T_e = 6500$–9000 K, where nearly all cooling is by [O III] $\lambda\lambda4959$–5007. The O II region extends from 6×10^{13} cm to $\sim 2 \times 10^{15}$ cm, where the major fraction of the ionizing energy is deposited. Because of the high metallicity, the temperature is only ~ 3500 K. The low temperature and high density explains the low luminosity of the [O II] lines. Instead, because of the high sulfur abundance, 0.044 by number, the [S III] $\lambda\lambda9069$–9532 lines are strong in the inner region. Between $\sim 1 \times 10^{15}$ cm and the O I Strömgren radius at $\sim 2 \times 10^{15}$ cm, there is a zone characterized by strong O I recombination lines. Outside, silicon and sulfur remain ionized because of their low ionization potentials. The total abundance of these ions is ~ 0.12, and the electron fraction stays constant at this level. This partially ionized zone extends throughout the whole oxygen core. The temperature is very low, ~ 3000 K at the inner boundary, decreasing to less than ~ 1000 K, and most of the emission from this region is from the [Si II] $\lambda34.81$ μm fine structure line. Recombination emission from Mg I] $\lambda4571$ is also important.

With regard to the total emitted spectrum, the most characteristic features of an oxygen-rich gas are the strong O I recombination lines in the ultraviolet, $\lambda\lambda1302$–1356, and in the optical, $\lambda7774$ and $\lambda8446$. The $\lambda8446$ line can also be strong in unprocessed gas because of fluorescence with Lyβ. The $\lambda7774$ line is not affected by this and can serve as an indicator of oxygen-rich gas. Both [S III] $\lambda\lambda9069$–9532 and [O III] $\lambda\lambda4959$–5007 are also expected to be strong. The latter line is a common feature of nearly all compositions containing even a small amount of oxygen. Because of the unusually low temperature in the O III region, the $\lambda\lambda4363/4959$–5007 ratio is expected to be considerably smaller than in unprocessed gas. If the density is higher than $\sim 10^8$ cm^{-3}, e.g., due to clumpimg, the [O III] lines can get optically thick and the ratio of the $\lambda4959$ and $\lambda5007$ lines can approach unity (Chevalier & Fransson 1992, in preparation). A high ratio is a strong indication that the gas is processed. A characteristic feature in the ultraviolet is strong oxygen lines with a wide range of ionization: O I $\lambda\lambda1300$–1356, O IV] $\lambda1400$, O V] $\lambda1217$, and O VI $\lambda1030$.

An interesting result is that the [O I] $\lambda\lambda6300$–6364 luminosity is very low in model MO, only $\sim 1.8 \times 10^{33}$ ergs s^{-1}, despite the presence of an extended O I zone. The reason is that fine structure cooling of especially [Si II] $\lambda34.81$ μm is dominant, with the result that a thermal instability occurs behind the ionization front, and the temperature in the O I zone is only 750–1300 K, which is too low for excitation of [O I] $\lambda\lambda6300$–6364. The high silicon abundance is not the main reason for this dominance of fine structure cooling, because it also occurs in other oxygen-dominated zones. The two main parameters determining whether the far-infrared lines dominate are the density and the form of the spectrum at high energies. If the density is considerably higher than in our models, e.g., because of clumping, fine structure cooling tends to become less important. In a model with a filling factor 0.1, i.e., a density enhancement by a factor 10, the ratio of the [O I] $\lambda\lambda6300$–6364 to the O I $\lambda7774$ line increased from 0.43 in the "standard" model to 3.4 in the clumped model. Lines from the ionized line regions are much less affected by the density increase. An increase in the heating of the partially ionized zone can also prevent the thermal instability. A spectrum flatter than our Crab spectrum has exactly this effect. A calculation with a ν^{-1} spectrum, but otherwise the same parameters, gave a fairly similar result for the highly ionized lines, with [S III] $\lambda\lambda9069$–9532 and [O III] $\lambda\lambda4959$–5007 as the strongest, while the O I recombination lines decreased substantially. The main difference was that the temperature of the O I region increased to ~ 3400 K behind the ionization front. This resulted in a large increase of the [O I] $\lambda\lambda6300$–6364 lines, with an [O I] $\lambda\lambda6300$–6364 to O I $\lambda7774$ ratio of 1.6.

When we compare the different models, the most apparent difference, except for the emitted spectrum, is the extent of the ionized zone, as already anticipated from the discussion in the last section (Fig. 1). While hydrogen has a large shielding efficiency, helium allows radiation below 24.5 eV to escape. The shielding efficiencies of carbon and oxygen are also low because of their high atomic weight. Radiation below 24.5 eV can therefore ionize the hydrogen-rich gas in the core or, if the hydrogen abundance in this region is low, the envelope. A realistic case with strong mixing may display a highly inhomogeneous structure with hydrogen-rich blobs having high ionization in their surface layers, and a relatively low ionization in their core regions, resembling the situation in the Crab Nebula (e.g., Davidson & Fesen 1985). Metal-rich blobs will in general be of higher ionization, unless their mass density is considerably higher than that of unprocessed gas.

The luminosity of the ionizing radiation is highly uncertain. We have calculated several additional models with different luminosities for the oxygen-dominated case. Varying the luminosity from 3×10^{37} ergs s^{-1} to 1×10^{40} ergs s^{-1} has a relatively minor effect on the emitted spectrum. In all cases the [S III] $\lambda\lambda9069$–9532, [O III] $\lambda\lambda4959$–5007, and O I $\lambda\lambda1300$–1356 lines were the strongest lines, each emitting $\sim 5\%$–10% of the ionizing luminosity. The main difference was the increasing importance of the highly ionized ultraviolet lines of O IV–VI with increasing luminosity. This conclusion also applies to a variation of the filling factor. This is expected because an increase in the density has the same effect on the ionization parameter as a decrease in the luminosity. Our results for the optical spectrum should therefore be relatively insensitive to these parameters and mainly depend on the composition.

TABLE 4

LUMINOSITIES[a] OF THE STRONGEST LINES AT 10 YR

MS		MHe		MO	
Lyα	1.83	C IV 1550	0.92	[S III] 9069–9532	0.86
C IV 1550	0.80	[Ne II] 12.81 μm	0.49	[O III] 4959–5007	0.49
[O III] 4959–5007	0.43	[Ne III] 3869–3968	0.26	O I] 1356	0.35
C III] 1909	0.29	C III] 1909	0.21	O VI 1034	0.32
Hα	0.15	[Ne V] 3346–3426	0.19	O V] 1216	0.31
[Ne III] 3869–3968	0.10	C II] 2326	0.17	[Ne II] 12.81 μm	0.27
O VI 1034	0.10	[O III] 4959–5007	0.16	O IV] 1400	0.18
O V] 1216	0.094	He I 10830	0.11	O I 1302	0.15
[Ne V] 3346–3426	0.085	[S III] 9069–9532	0.063	O I 7774	0.059
O III] 1664	0.077	[Ne III] 15.55 μm	0.048	O I 990	0.047
[O III] 4363	0.074	[Ne IV] 2423–2425	0.038	[Si II] 34.81 μm	0.036
[O I] 6300–6364	0.071	O VI 1034	0.013	O I 8446	0.021

[a] All luminosities in 10^{38} ergs s^{-1}.

2.6. *Time Dependence*

The discovery of an increasing number of old supernovae with ages more than 10 yr makes it interesting to examine the expected time evolution of the emission. For this reason we have calculated the same set of models as in § 2.5 for an age of 10 yr. The strongest lines are listed in Table 4.

While most of the strong lines at 10 yr are the same as at 1500 days, there are some important differences. As the density in the remnant decreases, forbidden lines increase in importance. This effect is mainly seen in the solar composition model, where the electron density is factor ~ 4 and ~ 10 higher than in the helium- and oxygen-dominated models, respectively. Collision de-excitation is important for the solar composition model at 4 yr, while the other models are already close to or below the critical density at this time. If clumping is important, quenching of the forbidden lines will also be important for the other models early, and an evolution toward a spectrum dominated by forbidden lines is also expected for these. An illustration of this can be seen in model MS where the [O III] $\lambda\lambda$4959–5007 and [Ne III] $\lambda\lambda$3869–3968 lines increase by a factor of ~ 10 from 4 to 10 yr, while the Lyα and C IV λ1550 lines remain nearly constant. The evolution of the line widths with time (Fig. 1) has already been discussed in § 2.4.

3. APPLICATIONS

3.1. *Observed Pulsar Nebulae*

The model described in the previous section can be best tested by comparing it to observed nebulae known to contain young pulsars. The most favorable such cases are the nebulae associated with PSR 0531+21 (Crab Nebula), PSR 0540−69, and PSR 1509−58 (MSH 15−52); Table 5 summarizes the information that is available on these pulsars. The observed parameters are the period, P, the period derivative, $\dot{P}$, and the braking index, b, and are from Lyne, Pritchard, & Smith (1988) for PSR 0531+21, Manchester & Peterson (1989) for PSR 0540−69, and Manchester, Durdin, & Newton (1985) for PSR 1509−58. The derived parameters $t + \tau$, L_0, and initial period P_0 assume evolution with constant magnetic moment and braking index (see eq. [2.5]). The neutron star moment of inertia is $I = I_{45}\,10^{45}$ g cm^2 and we assume $I_{45} = 1$ here. A set of neutron star models by Arnett & Bowers (1977) with precollapse masses of 1.41 $M_\odot$ have values of I within a factor of 2 of this value. We have $L \propto I$, so that varying I can be accomplished with the scaling relations given below. The age of 0531+21 is determined by the time of SN 1054, and the age of 0540−69 is determined by the expansion velocity and size of the optical remnant. The value of τ for PSR 1509−58 is determined from the model described below. The pulsar properties give the quantities for $L(t)$ (eq. [2.5]), which is then substituted into equation (2.4).

The model described here is similar to that proposed by Chevalier (1977). As in that work, we presume that the mixture of H and He observed in the Crab is the result of hydrodynamic instabilities between the He mantle and the H envelope during the explosion. The main difference between the models is in the assumed density profile for the freely expanding supernova gas. Here we assume a continuous density structure so that the nebula is still running into supernova material at the present time. Because the age is $\geq \tau$, it is necessary to integrate equations (2.3) and (2.4) numerically. The constant L_0 solutions provide the initial conditions. We assume that radiative losses in the pulsar bubble can be neglected, although in the case of the Crab Nebula, the current luminosity is $\sim 1.6 \times 10^{38}$ ergs s^{-1} (Davidson & Fesen 1985), or $\sim \frac{1}{3}$ of the total pulsar output with $I_{45} = 1$. The evolution of the radiative losses is unknown, so it is not possible to realistically include these losses in the calculations. If the losses are proportional to L, then their effect is the same as a change in I; neglect of losses in the Crab is equivalent to taking $I_{45} = 1.35$.

Although completely analytic solutions are not possible for the types of models described in this section, scaling laws apply once values of m, n, and τ have been specified. They are

$$R \propto V \propto M_t^{-1/2} E^{(3-m)/2(5-m)} L^{1/(5-m)} , \tag{3.1}$$

$$\rho_e \propto M_t^{5/2} E^{-5(3-m)/2(5-m)} L^{-m/(5-m)} , \tag{3.2}$$

$$E_{\rm kin} \propto E_{\rm int} \propto M_t^0 E^0 L^1 . \tag{3.3}$$

TABLE 5

OBSERVED PULSARS IN NEBULAE

Parameter	PSR 0531+21	PSR 0540−69	PSR 1509−58
Nebulae	Crab	0540−69	MSH 15−52
P (s)	0.0333	0.0503	0.150
$\dot{P}$	4.21×10^{-13}	4.77×10^{-13}	1.54×10^{-12}
b	2.509	2.01	2.83
L (ergs s^{-1})	4.5×10^{38}	1.5×10^{38}	1.8×10^{37}
$t + \tau$ (yr)	1660	3310	1690
t (yr)	930	830	1660
τ (yr)	730	2480	30
L_0 (ergs s^{-1})	3.0×10^{39}	3.5×10^{38}	8.3×10^{40}
P_0 (s)	0.019	0.038	0.017
β	1.3	0.75	2.1

Results of Crab Nebula models with several density distributions are given in Table 6. All the models use $n = 9$, $M_t = 10\ M_\odot$, and $E = 1 \times 10^{51}$ ergs to describe the supernova density distribution; only the power-law index, m, for the inner density profile is varied. The observed quantities are from the review by Davidson & Fesen (1985) unless otherwise mentioned, and the distance to the Crab Nebula is taken to be 2 kpc. The quantity $v_{\rm sh}$ is the relative velocity of the shock front moving into the supernova gas and $t_{\rm cool}$ is the cooling time for the shocked gas. The comparisons of the models and observations of R and V are complicated by the fact that the nebula is not spherical and that many of the dense filaments are well inside the outer boundary, presumably because of the Rayleigh-Taylor instability. If the instability were allowed to occur in the models, the outer boundary would be larger than that given. The observed value of $t - R/V$ has been measured to be 86 yr (Trimble 1968) and 66 ± 7 yr (Wyckoff & Murray 1977) from optical studies, and 179 yr (whole nebula) and 203 yr (outer edge) from radio studies (Bietenholz et al. 1991). These observations give direct evidence for acceleration by the pulsar nebula. The observed minimum pressure in relativistic particles and magnetic fields is determined by Wilson, Samarasinha, & Hogg (1985) for the base of the Crab Nebula jet.

The models show general agreement with the basic observed features of the Crab Nebula. One difference with models in which there is a stationary external medium is that in the present case there is a small acceleration at the outer boundary and certainly no deceleration. Radio observations of the outer nebula (Bietenholz et al. 1991) and optical observations of the outer jet (Shull et al. 1984; Marcelin et al. 1990) show no evidence for deceleration. While this is consistent with the present model, it may also be consistent with a low external density, ≤ 0.05 cm^{-3}, in a stationary external medium (Bietenholz et al. 1991).

The accelerating shell drives a shock front into the freely expanding supernova gas, with the shock velocity and preshock density given in Table 6. These parameters can be used to calculate the cooling time for the postshock gas, which is also given in the table. These estimates assume normal cosmic abundances. Helium is overabundant in the Crab Nebula, but it does not contribute significantly to the radiative cooling; the heavier elements, which are important, appear to have fairly normal mass fractions. It can be seen that the cooling time is somewhat longer than the age at present so that the gas currently remains hot, at a temperature of about 7×10^5 K. The gas is too cool to emit significant X-ray emission, which is consistent with observed upper limits on such emission (Schattenburg et al. 1980). A possible problem is that the lack of cooling implies that gas is not currently being added to the cool filaments and thus does not contribute to the observed filament mass. The model mass may then be less than the observed mass.

In the present model, the filamentary structure of the Crab Nebula is due to the action of the Rayleigh-Taylor instability discussed in § 2.4, where it was found that the instability is expected to grow for $l \geq 4$. In the nonlinear limit, the largest scales that can grow are expected to be the dominant ones. The observed filamentary network in the Crab Nebula (Clark et al. 1983) is consistent with this hypothesis.

A consequence of the present model, as of that discussed by Chevalier (1977), is that the observed Crab Nebula is surrounded by freely expanding supernova ejecta, beyond which is a fast shock wave moving into the ambient medium. Murdin & Clark (1981) have found evidence for a faint Hα halo that may be from such ejecta, but the result remains unconfirmed. The large extent of the emission ($6' \times 14'$ in radius) and its high degree of ellipticity are surprising properties in the context of the present model. Evidence for a fast shock wave around the Crab Nebula is lacking. Although the most stringent limits are probably at radio wavelengths, they can still accommodate a fast shock if the shock front is moving into a low-density gas, as expected in a stellar wind bubble created by the massive progenitor star (Chevalier 1985). Romani et al. (1990) have in fact found evidence for a large shell around the Crab Nebula at infrared and 21 cm wavelengths; the shell radius, 90 pc at the distance of the Crab Nebula, is surprisingly large.

For the nebula with many features in common with the Crab Nebula, 0540−69, there is evidence for the fast shock front. Mathewson et al. (1980) found that [O III] imaging showed an arc 30″ west of a small nebula 4″ in radius. A radio image of the region with the Australia Telescope by Kesteven, Manchester, & Staveley-Smith (1991) shows emission both from the central nebula and from the arc, which strongly suggests that the arc is a shock front. At a distance of 50 kpc, the radius of the arc is 7.3 pc and the average velocity to that distance is 8600 km s^{-1} for an age of 830 yr. The arc is part of the shell that is observed in the radio image.

Unlike the Crab Nebula, the age of the 0540−69 nebula is not known, but the observed ratio R/V gives a time scale of 690 yr for distance of 50 kpc (Mathewson et al. 1980; Kirshner et al. 1989). Table 7 shows the results of a model with an age of 830 yr that has the appropriate time scale R/V. The supernova model used for this case has $m = 1$, $n = 9$, $M_t = 10\ M_\odot$, and $E = 1 \times 10^{51}$ ergs. The large apparent abundance of oxygen in 0540−69 suggests that the initial stellar mass was greater than $10\ M_\odot$, but a Type Ib progenitor is also a possibility, which would indicate a smaller mass. Model results for a different value of M_t can be found from the above scaling laws. The

TABLE 6

CRAB NEBULA MODELS AT $t = 930$ yr

Parameter	$m = 0$	$m = 1$	$m = 2$	Observed
R (pc)	1.7	1.4	0.99	1.6×2.1
V (km s^{-1})	2000	1700	1300	
$t - R/V$ (yr)	110	130	160	66–200
M ($M_\odot$)	1.1	1.3	2.0	2–3
$E_{\rm int}$ (ergs)	1.1×10^{49}	1.1×10^{49}	1.0×10^{49}	
$E_{\rm kin}$ (ergs)	4.5×10^{49}	3.8×10^{49}	3.1×10^{49}	4×10^{49}
p_i (dynes cm^{-2})	5.8×10^{-9}	1.0×10^{-8}	2.9×10^{-8}	$\geq 9 \times 10^{-9}$
$v_{\rm sh}$ (km s^{-1})	230	240	220	
ρ_e (g cm^{-3})	3.4×10^{-24}	4.7×10^{-24}	1.1×10^{-23}	
$t_{\rm cool}$ (yr)	5600	4500	1500	

TABLE 7

0540−69 MODEL AT $t = 830$ yr

Parameter	Model	Observed
R (pc)	0.77	0.97
V (km s^{-1})	1100	1370
R/V (yr)	690	690
M ($M_{\odot}$)	0.46	
$E_{\rm int}$ (ergs)	2.3×10^{48}	
$E_{\rm kin}$ (ergs)	5.6×10^{48}	
p_i (dynes cm^{-2})	1.3×10^{-8}	
$v_{\rm sh}$ (km s^{-1})	190	
ρ_e (g cm^{-3})	1.1×10^{-23}	
$L_{\rm rad}$ (ergs s^{-1})	2.6×10^{36}	$\geq 2 \times 10^{35}$

TABLE 8

MSH 15−52 MODEL AT $t = 1660$ yr

Parameter	Model	Observed
R (pc)	3.7	3.7×6.1
V (km s^{-1})	2200	
R/V (yr)	1600	
M ($M_{\odot}$)	2.6	
$E_{\rm int}$ (ergs)	3.1×10^{48}	
$E_{\rm kin}$ (ergs)	1.3×10^{50}	
p_i (dynes cm^{-2})	1.7×10^{-10}	
$v_{\rm sh}$ (km s^{-1})	59	
ρ_e (g cm^{-3})	5.8×10^{-25}	
$L_{\rm rad}$ (ergs s^{-1})	9.5×10^{34}	

observed values of R and V are taken from Mathewson et al. (1980) and Kirshner et al. (1989). It is clear that slight variation of the various parameters (including I_{45}) could bring even better agreement with the observations, but that the basic properties of the remnant are reproduced. Our model for 0540−69 is close to the models considered by Reynolds (1985).

Table 7 also gives the conditions at the shock front that is driven into the supernova gas. An important difference with the Crab Nebula is that the gas is apparently O-rich, so that the cooling of the gas is significantly enhanced. Detailed models are necessary for the shock emission because it is strongly out of ionization equilibrium. Itoh (1981) has calculated models for shock waves moving into a pure O gas and finds that for a shock velocity of 141.4 km s^{-1} and an ambient heavy-element density of 1 cm^{-3}, the cooling time for the postshock gas is about 10 yr. The ambient density for the case shown in Table 7 is 0.4 cm^{-3}, so that the expected cooling time is less than the age of the remnant provided that the slightly higher shock velocity does not cause a large change in cooling properties. If the shock is cooling, the quantity $L_{\rm rad}$ is available to be radiated and it is larger than the observed luminosity in optical emission lines. Itoh (1981) finds that for a shock velocity of 141.4 km s^{-1} much of the radiative luminosity is emitted in optical lines. Kirshner et al. (1989) have already proposed that the optical line emission from 0540−69 is from a shock front based on the high [O III] temperature and on the fact that the ionization parameter appears to be low in this remnant. If the present shock model is correct, the morphology of the remnant may be different from that of the Crab Nebula. Although some irregularities are likely to be present, the nebula should appear less filamentary than the Crab. Although the [O III] image by Mathewson et al. (1980) gives some evidence in this direction, high-resolution imaging is needed.

While the Crab Nebula and 0540−69 have age estimates independent of their central pulsars, that is not the case for MSH 15−52. A small value of τ is taken here (Tables 5 and 8) so that the nebula can grow to a large size, despite the present rather small power output from the pulsar. The size has been derived for the X-ray synchrotron nebula by Seward et al. (1984) and is given in Table 8. The model listed in Table 8 has the same supernova model as that for 0540−69 and the $m = 1$ model for the Crab Nebula. The large size results in a small internal pressure, which is also inferred from the X-ray observations. Another property of the early injection of energy is that the acceleration occurs early in the evolution and the shell is now close to free expansion. For cosmic abundances and the shock parameters given in Table 8, the shock front is close to the transition to nonradiative evolution. Even if the shock front is still radiative, the radiative luminosity is small. No optical nebula has yet been observed around the synchrotron nebula. For the conditions predicted here, the [O I] λ6300 line may be most appropriate for a shell search.

Another advantage of a small value for τ is that the age of the remnant is maximized so that there is sufficient time to produce the large nebula with a radius of 18 pc observed at X-ray, optical, and radio wavelengths (Seward et al. 1983). For an age of 1660 yr, an average velocity of 10,600 km s^{-1} is involved in creating the nebula. Such rapid expansion is plausible if the remnant has been expanding in a low-density stellar wind bubble and is now beginning to interact with a wind-created shell (Chevalier & Liang 1989). Low velocities are observed in the optical emission because the emission is due to slow radiative shocks being driven into dense shell gas.

Two other nebulae with associated pulsars are the Vela remnant and CTB 80. Both of these objects are fairly old and appear to involve interaction with the interstellar medium. Another class of objects show synchrotron nebulae like the Crab Nebula (e.g., 3C 58), but do not have directly observed pulsars. Although the present theory may apply to some of these objects, there are generally not enough observational constraints for informative comparisons.

3.2. *Supernovae*

The other aim here is to examine whether younger objects show evidence for pulsar excitation even though a pulsar is not directly observed. We assume that the ages are $t \ll \tau$ so that the theory developed in § 2 for constant L applies. An obvious candidate is SN 1987A, which provides a strong test for the presence of a pulsar because of its proximity. Fransson & Chevalier (1987) and Colgan & Hollenbach (1988) have already discussed the fact that highly ionized atoms would be expected from photoionization by a pulsar nebula. Sato & Yamada (1991) considered pulsar bubble models of the type described here and noted that the radiative efficiency could be small. They also considered the radiative output for the density profile from a specific one-dimensional model for the supernova. Here we assume that instabilities will be able to smooth the density profile so that the density profile is as described above; the observed line profiles for SN 1987A do not indicate the presence of a shell.

Suntzeff et al. (1992) find that a central pulsar can be contributing no more than $\sim 8 \times 10^{36}$ ergs s^{-1} to the ultraviolet through infrared luminosity of SN 1987A on day 1500. Any pulsar bubble must still be in the radiative phase; for a radiative luminosity of $0.015L$ (Table 1), the maximum pulsar power output is 5×10^{38} ergs s^{-1}. From equations (2.10) and (2.11), the maximum shell velocities are hundreds of km s^{-1}. The best way to search for pulsar effects may be to search for line emission with this characteristic Doppler width; it should be present even if the radiative efficiency of the pulsar bubble itself is small.

If a pulsar bubble with a high radiative efficiency is present in SN 1987A, our discussion in § 2.5 shows that the emission depends sensitively on the chemical composition close to the bubble. If the gas is oxygen-rich, the [O III] $\lambda\lambda$4959–5007 is expected to have a luminosity $\sim$5%–10% of the total ionizing luminosity. If there is also a high sulfur abundance in this zone, as indicated by models, the [S III] $\lambda\lambda$9069–9532 lines are expected to have a similar luminosity. Except for the narrow circumstellar emission, no [O III] emission is seen in the spectra of SN 1987A. As a rough upper limit we take 50% of the [O I] $\lambda\lambda$6300–6364 luminosity on day 806 from the spectra in Phillips & Williams (1991). This gives an upper limit of an $\sim 5 \times 10^{35}$ ergs s^{-1} to the [O III] emission. Assuming an efficiency of $\sim$5%, this results in an upper limit of $\sim 1 \times 10^{37}$ ergs s^{-1} for the ionizing continuum from a central pulsar nebula. A similar limit is obtained from the [S III] $\lambda\lambda$9069–9532 line. The presence of dust, as well as a composition dominated by iron group elements, in the inner regions could make this limit less stringent. However, the limit is comparable to that from the bolometric luminosity (Suntzeff et al. 1992). Our analysis emphasizes ultraviolet through infrared line radiation; Woosley, Pinto, & Hartmann (1989) have discussed the hard X-ray radiation that might be expected from a pulsar nebula.

The models can be applied to late observations of other supernovae. The problem is that circumstellar interaction is another possible source of optical emission and could be confused with pulsar emission. Supernovae that have been optically observed at late times (e.g., Leibundgut et al. 1991) also show radio emission, which indicates that circumstellar interaction is taking place. Chevalier (1987) suggested that pulsar emission could be occurring in SN 1986J because of the narrow line profiles. The suggestion was initially based on the narrow H and He lines, but observations of other supernovae, like SN 1988Z (Stathakis & Sadler 1991), show that narrow H lines can occur early when the inner regions are still optically thick. Some type of circumstellar excitation is indicated for these lines, which implies that narrow line emission is not necessarily from slow, central gas that is excited by a pulsar nebula. If there is ambiguity about the excitation source, a strong prediction of the pulsar nebula model is that the velocities of the emitting gas should be found to increase with time.

4. DISCUSSION AND SUMMARY

The aim of this paper is to present a unified picture for the appearance of a pulsar nebula that is interacting with surrounding supernova gas. A minimum amount of luminosity is produced by the shock front that is driven into the supernova gas; this is generally about 1.5% of the total supernova power. Additional luminosity can be produced by emission from within the pulsar bubble and we consider the emission from supernova gas that is excited by a central pulsar nebula.

The dynamical model can be tested by observations of nebulae known to contain young pulsars. The Crab Nebula is a well-observed case, but is one in which the external supernova gas has not been detected so that the basic model remains to be confirmed. The expectation is for cool, photoionized gas surrounding the Crab Nebula (possibly observed by Murdin & Clark 1981) and for a fast shock front at larger radii. The fast shock would be best observed by nonthermal radio emission. The presence of an outer fast shock front and an inner pulsar nebula is clearly seen in the radio observations of 0540−69 (Kesteven, Manchester, & Staveley-Smith 1991). We suggest that the central optical emission in this case is produced by a shock front driven into the freely expanding ejecta by the pulsar bubble. A prediction of the model is that the optical morphology should be less filamentary than that of the Crab Nebula, which is composed of swept-up photoionized gas that has undergone a Rayleigh-Taylor instability. The third nebula, MSH 15−52, has relatively little data available on the pulsar nebula, except at X-ray wavelengths (Seward et al. 1984). A small value was chosen for the pulsar τ in this case so that the early energy deposition is able to create a fast shell nebula, as is indicated by the size of the X-ray emitting region. This also has the effect of giving a relatively weak inner shock front at the present time (no such shock emission has been observed) and of maximizing the age of the remnant, which may be needed to produce the large-scale supernova remnant. This model requires a powerful initial pulsar, with a power output close to 1×10^{41} ergs s^{-1}. The reason for the large L_0, and the small τ, is a strong pulsar magnetic field; the estimated initial period is close to that for the Crab pulsar. A prediction of our model is the presence of a shell around the X-ray pulsar nebula; it may be a source of weak optical shock emission.

The modeling of pulsar nebulae gives some information of the history of the central pulsar power output. For the Crab Nebula and 0540−69, the pulsar cannot have become active very recently, but must have an age comparable to the age of the supernova. However, it is possible that the pulsars became active years or tens of years after the supernova explosion. Observations of supernovae in this age range are needed to determine whether active pulsars are present. When the minimum shock luminosity argument is applied to SN 1987A, the upper limit on the current pulsar power is 5×10^{38} ergs s^{-1}. Our spectral models make specific predictions for the signature of a pulsar nebula at an age of up to tens of years. A general prediction is the acceleration of the emitting gas by the pulsar nebula. Observational studies of Type II supernovae at late times should certainly be carried out, but a substantial investment of telescope time is required because the nebulae are likely to be faint. The payoff may be a better understanding of early pulsar evolution.

R. A. C.'s research was supported in part by NSF grants AST-8818362 and AST-9016687.

REFERENCES

Arnett, W. D. 1988, ApJ, 331, 377

Arnett, W.D., & Bowers, R. L. 1977, ApJS, 33, 415

Bandiera, R., Pacini, F., & Salvati, M. 1984, ApJ, 285, 134

Bietenholz, M. F., Kronberg, P. P., Hogg, D. E., & Wilson, A. S. 1991, ApJ, 373, L59

Blandford, R. D., Applegate, J., & Hernquist, L. 1983, MNRAS, 204, 1025

Borkowski, K. J., & Shull, J. M. 1990, ApJ, 348, 169

Chevalier, R. A. 1977, in Supernovae, ed. D. N. Schramm (Dordrecht: Reidel), 53

———. 1984, ApJ, 280, 797

———. 1985, in The Crab Nebula and Related Supernova Remnants, ed. M. C. Kafatos & R. Henry (New York: Cambridge Univ. Press), 63

Chevalier, R. A. 1987, Nature, 329, 611

———. 1989, ApJ, 346, 847

———. 1991, in SN 1987A and Other Supernovae, ed. I. J. Danziger (Garching: ESO), 511

Chevalier, R. A., & Liang, E. P. 1989, ApJ, 344, 332

Chevalier, R. A., & Soker, N. 1989, ApJ, 341, 867

Clark, D. H., Murdin, P., Wood, R., Gilmozzi, R., Danziger, J., & Furr, A. W. 1983, MNRAS, 204, 415

Colgan, S. W. J., & Hollenbach, D. J. 1988, ApJ, 329, L25

Colgate, S. A. 1971, ApJ, 163, 221

Davidson, K., & Fesen, R. A. 1985, ARA&A, 23, 119

Emmering, R. T., & Chevalier, R. A. 1987, ApJ, 321, 334

Emmering, R. T., & Chevalier, R. A. 1989, ApJ, 345, 931

Fransson, C., & Chevalier, R. A. 1985, ApJ, 296, 35

———. 1987, ApJ, 322, L15

———. 1989, ApJ, 343, 323

Fryxell, B., Müller, E., & Arnett, W. D. 1991, ApJ, 367, 619

Gaffet, B. 1977, ApJ, 216, 565

Herant, M., & Benz, W. 1992, ApJ, 387, 294

Itoh, H. 1981, PASJ, 33, 1

Kennel, C. F., & Coroniti, F. V. 1984a, ApJ, 283, 694

———. 1984b, ApJ, 283, 710

Kesteven, M. J., Manchester, R. N., & Staveley-Smith, L. 1991, in IAU Symp. 148, The Magellanic Clouds, ed. R. Haynes & D. Milne (Dordrecht: Kluwer), 323

Kirshner, R. P., Morse, J. A., Winkler, P. F., & Blair, W. P. 1989, ApJ, 342, 260

Kozma, C., & Fransson, C. 1992, ApJ, 390, 602

Leibundgut, B., Kirshner, R. P., Pinto, P. A., Rupen, M. P., Smith, R. C., Gunn, J. E., & Schneider, D. P. 1991, ApJ, 372, 531

Lyne, A. G., Pritchard, R. S., & Smith, F. G. 1988, MNRAS, 233, 667

Manchester, R. N., & Peterson, B. A. 1989, ApJ, 342, L23

Manchester, R. N., Durdin, J. M., & Newton, L. M. 1985, Nature, 313, 374

Marcelin, M., Véron-Cetty, M. P., Woltjer, L., Boulesteix, J., d'Odorico, S., & Lecoarer, E. 1990, A&A, 228, 471

Mathewson, D. S., Dopita, M. A., Tuohy, I. R., & Ford, V. L. 1980, ApJ, 242, L73

McKee, C. F., & Hollenbach, D. 1980, ARA&A, 18, 219

Middleditch, J., & Kristian, J. 1984, ApJ, 279, 257

Murdin, P., & Clark, D. H. 1981, Nature, 294, 543

Narayan, R., & Ostriker, J. P. 1990, ApJ, 352, 222

Nussbaumer, H., & Storey, P. J. 1984, A&AS, 56, 293

Ostriker, J. P., & Gunn, J. E. 1971, ApJ, 164, L95

Phillips, M. M., & Williams, R. E. 1991, in Supernovae, Proc. 10th Santa Cruz Summer Workshop in Astronomy and Astrophysics, ed. S. E. Woosley (Berlin: Springer) 36

Rees, M. J., & Gunn, J. E. 1974, MNRAS, 167, 1

Reynolds, S. P. 1985, ApJ, 291, 152

Reynolds, S. P., Chevalier, R. A. 1984, ApJ, 278, 630

Romani, R. W., Reach, W. T., Koo, B. C., & Heiles, C. 1990, ApJ, 349, L51

Sato, H., & Yamada, Y. 1991, Prog. Theor. Phys., 85, 541

Schattenburg, M. L., Canizares, C. R., Berg, C. J., Clark, G. W., Markert, T. H., & Winkler, P. F. 1980, ApJ, 241, L151

Seward, F. D., Harnden, F. R., Jr., Murdin, P., & Clark, D. H. 1983, ApJ, 281, 650

Seward, F. D., Harnden, F. R. Jr., Szymkowiak, A., & Swank, J. 1984, ApJ, 267, 698

Seward, F. D., & Wang, Z. 1988, ApJ, 332, 199

Shigeyama, T., & Nomoto, K. 1990, ApJ, 360, 242

Shull, P., Carsenty, U., Sarcander, M., & Neckel, T. 1984, ApJ, 285, L75

Stathakis, R. A., & Sadler, E. M. 1991, MNRAS, 250, 786

Suntzeff, N. B., Phillips, M. M., Elias, J. H., Depoy, D. L., & Walker, A. R. 1992, ApJ, 384, L33

Trimble, V. L. 1968, AJ, 73, 535

Vishniac, E. T. 1983, ApJ, 274, 152

Weaver, R., McCray, R., Castor, J., Shapiro, P. R., & Moore, R. T. 1977, ApJ, 218, 377

Weaver, T., & Woosley, S. E. 1980, in Supernovae Spectra, ed. R. Meyerott & G. H. Gillespie (New York: AIP), 15

Weiler, K. W., Sramek, R. A., Panagia, N., van der Hulst, J. M., & Salvati, M. 1986, ApJ, 301, 790

Wilson, A. S., Samarasinha, N. H., & Hogg, D. E. 1985, ApJ, 294, L121

Woosley, S. E. 1988, ApJ, 330, 218

Woosley, S. E., Pinto, P. A., & Hartmann, D. 1989, ApJ, 346, 395

Wyckoff, S., & Murray, C. A. 1977, MNRAS, 180, 717